Blue laser emission by intracavity second harmonic generation in Nd:ASL pumped by a tapered amplifier laser diode stabilized by a volume Bragg grating

David Pabœuf, Gaëlle Lucas-Leclin, Patrick Georges, Bernd Sumpf, Götz Ebert, Cyrille Varona, Pascal Loiseau, Gérard Aka, Bernard Ferrand

Blue laser emission by intracavity second harmonic generation in Nd:ASL pumped by a tapered amplifier laser diode stabilized by a volume Bragg grating

David Pabœuf[1], Gaëlle Lucas-Leclin[1], Patrick Georges[1], Bernd Sumpf[2], Götz Ebert[3], Cyrille Varona[3], Pascal Loiseau[3], Gerard Aka[3], Bernard Ferrand[4]

1 Laboratoire Charles Fabry de l'Institut d'Optique, CNRS, Univ. Paris-Sud, RD128, 91127 Palaiseau, France
2 Ferdinand-Braun-Institut für Höchstfrequenztechnik, Albert-Einstein-Strasse 11, 12489 Berlin, Germany
3 Laboratoire de Chimie de la Matière Condensée de Paris, CNRS, ENSCP, 11 rue P. et M. Curie, 75231 Paris, France
4 Laboratoire de Cristallogenèse Appliquée, CEA – LETI, 17 Rue des martyrs, 38054 Grenoble, France

ABSTRACT We present the diode pumping of a Nd:ASL ($Sr_{1-x}La_{x-y}Nd_yMg_xAl_{12-x}O_{19}$) crystal for second harmonic generation at 453 nm. We have developed a high-brightness pump source based on a tapered amplifier in an extended cavity with a volume Bragg grating for wavelength stabilization. A pump brightness of 110 MW cm^{-2} sr^{-1} is obtained with a linewidth lower than 80 pm at 798 nm. This laser source is used to pump a Nd:ASL crystal to obtain 300 mW at 906 nm and 53 mW at 453 nm by intracavity doubling with a LBO crystal.

PACS 42.55.Xi; 42.55.Px; 42.65.Ky

1 Introduction

Diode-pumped solid-state lasers operating in the blue spectral range have a large number of applications ranging from high-density optical data storage to phototherapy and medical diagnostics. One way to design such a laser is to perform nonlinear conversion of a near infrared laser line. The neodymium $^4F_{3/2} \rightarrow {}^4I_{9/2}$ laser transition is one of the most used for the initial infrared source since it allows emission around 900 nm [1]. The development of high power diode laser sources around 808 nm to pump Nd-doped crystals has permitted the realization of compact and efficient lasers in the blue range. For instance, infrared laser operation and frequency doubling have been demonstrated with Nd:YAG (3 W at 473 nm for 22 W of pump power [2]), Nd:YVO_4 (4.5 W at 457 nm for 30 W incident pump power) [3] and Nd:$GdVO_4$ (220 mW at 456 nm for 2 W of pump power [4]) In order to reach deeper blue wavelengths, two ways are possible. The first way is to design a cavity emitting on a deeper Stark sub-level with a conventional Nd-doped crystal; quasi-three-level laser emission at 899 nm in Nd:YAG has indeed been recently demonstrated [5]. Another solution consists in developing new Nd-doped laser materials; among them, the Nd-doped strontium and lanthanum aluminate crystal $Sr_{1-x}La_{x-y}Nd_yMg_xAl_{12-x}O_{19}$ (Nd:ASL) seems to be promising since its quasi-three-level transition is located at 900 nm, which is one of the lowest for Nd-doped crystals [6]. Unfortunately, the absorption transitions of Nd:ASL are narrow-band (< 3 nm) and located at 792 nm and 798 nm (see Fig. 1) where commercial high power laser diodes are difficult to find. Moreover the quasi-three-level operation of the laser implies that the lower level of the laser transition is thermally populated. A bright enough pump source is then required to exceed the transparency intensity, evaluated to 3 kW cm^{-2}, and get a positive gain. Efficient infrared emission has already been demonstrated under Ti:sapphire pumping: in a quasi-two-level configuration, 950 mW at 901 nm have been obtained for 1.6 W of absorbed pump power at 865 nm [7]; up to 1.67 W of infrared laser at 900 nm have been demonstrated for 2.5 W absorbed power at 792 nm with a 5-mm long crystal in [8]. Furthermore, intracavity doubling with a BiBO crystal produced 320 mW of blue laser power at 450 nm. In view of these results, the demonstration of a diode-pumped Nd:ASL laser would be an interesting improvement in terms of compacity and wall-plug efficiency. To this purpose, we have developed our own high-brightness wavelength-stabilized pumping source at 798 nm based on a semiconductor tapered amplifier in extended cavity with a volume Bragg grating. In this paper, we report on the design and characteristics of this pumping source and its use for infrared laser emission of a Nd:ASL crystal together with intracavity second harmonic generation in a compact and efficient setup.

2 Design and characterization of the pumping source

The taper design is promising to achieve high brightness with a laser diode. It consists of a ridge section for spatial filtering and a tapered one for amplification. Very high powers have been demonstrated in diffraction limited beam (4.4 W at 808 nm [9], 8 W at 976 nm [10]). Secondly, volume Bragg gratings (VBG) have appeared to become essential optical components in the recent years, with a high spectral selectivity, low losses and reflectivity from a few % to

✉ Fax: +33 1 64 53 31 01, E-mail: david.paboeuf@institutoptique.fr

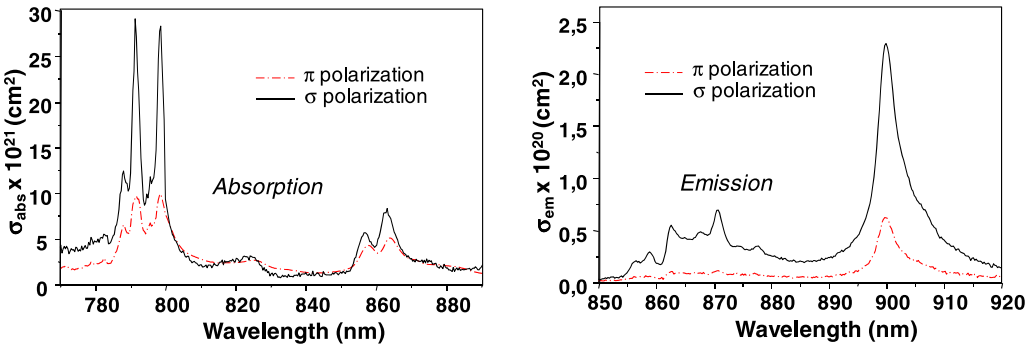

FIGURE 1 Absorption and emission spectra of Nd:ASL

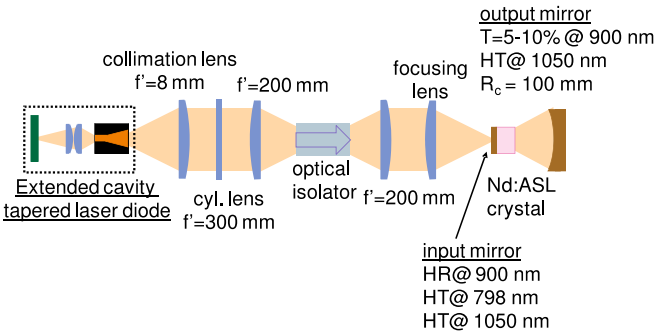

FIGURE 2 Experimental setup for cw 900 nm emission of Nd:ASL

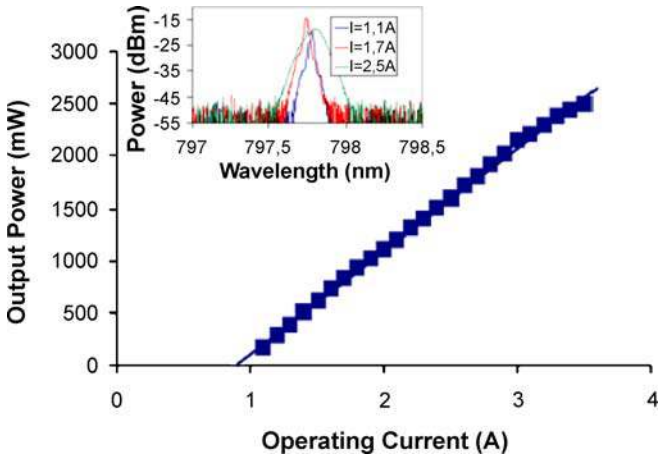

FIGURE 3 Laser performance of the extended cavity tapered laser. *Inset*: spectrum for different operating currents

100%. The major use of these components is the wavelength stabilization of laser diodes [11] or solid-state lasers [12]. The combination of a tapered amplifier and a VBG in an extended cavity would permit both high brightness and high spectral purity.

As the gain medium of our pumping source, we have used a tapered amplifier grown and designed at Ferdinand Braun Institut für Höchstfrequenztechnick for emission around 800 nm [9]. The active region of the tapered amplifier is composed of a tensile-strained GaAsP single quantum well embedded in a 3-μm thick $Al_{0.45}Ga_{0.55}As$ waveguide and highly doped $Al_{0.7}Ga_{0.3}As$ cladding layers. The index-guided straight ridge section is 2 mm long and the gain-guided tapered section is characterized by a tapered angle of 4° and a length of 2 mm. The front tapered facet of the amplifier has a reflectivity of 0.5%, whereas the rear facet reflectivity is about 0.1%. Without any optical feedback, only amplified spontaneous emission centered around 800 nm and covering a large spectral band (30 nm) is observed from this source. The VBG has a reflectivity of 20% at 798 nm and a spectral bandwidth of 200 pm. It is used as the back mirror of the extended cavity (see Fig. 2). The beam from the ridge side is focused into the grating, resulting in a better stability and a very low sensitivity to misalignments [13]. Regardless of operating current and temperature, the laser emission is locked on the Bragg wavelength with a very low wavelength drift that remains within the VBG spectral bandwidth. The side-mode suppression ratio is about 40 dB and the FWHM-linewidth is less than 80 pm (limited by the optical spectrum analyzer resolution). The threshold of the extended cavity laser diode is 1 A and the slope efficiency reaches 0.9 W A^{-1}. A maximum output power of 2.5 W is obtained for an operating current of 3.5 A (see Fig. 3). The beam quality parameter (M^2) is as good as 1.2 in both directions for an operating current of 2.5 A. At higher operating currents we observe a degradation of the beam quality and measure a M^2 around three in the slow axis direction. The steadiness of the beam quality with operating current could be improved by including higher isolation from optical feedback in the setup. Moreover, the relatively low reflection from the ridge side may result in an incomplete saturation of the tapered amplifier section [13]. Despite this slight beam degradation at high power, our extended cavity laser results in a compact and efficient high-brightness source fully suitable for solid-state laser pumping applications.

3 Optimization of the infrared operations

Reabsorption at the oscillating wavelength is the main challenge we face with quasi-three-level lasers. The available pump power being limited, the pump beam has to be strongly focused inside the crystal to reach a high intensity at the waist position. This leads to a very divergent pump beam which may limit the laser efficiency. Simulations have been carried out to evaluate the gain inside the crystal and determine the theoretically adequate parameters. The small signal gain integrated on the transverse section of the crystal can be written as [16]:

$$g_0(z) = \int_0^{r_c} N \frac{\sigma_{eL}\sigma_{aP} I_p(r,z) h\nu_p - \sigma_{aL}/\tau}{\sigma_{aP} I_p(r,z) h\nu_p - 1/\tau} \times A(r,z)\,\mathrm{d}r\,, \qquad (1)$$

σ_{eL} at 900 nm (cm^2)	σ_{aL} at 900 nm (cm^2)	σ_{eL} at 906 nm (cm^2)	σ_{aL} at 906 nm (cm^2)	σ_{aP} (cm^2)	τ (μs)	N (cm^{-3})
2.3×10^{-20}	4×10^{-21}	7×10^{-21}	5×10^{-22}	2.8×10^{-20}	380	1.7×10^{20}

TABLE 1 Spectroscopic data of Nd:ASL at $\lambda_L = 900$, and 906 nm and $\lambda_p = 798$ nm

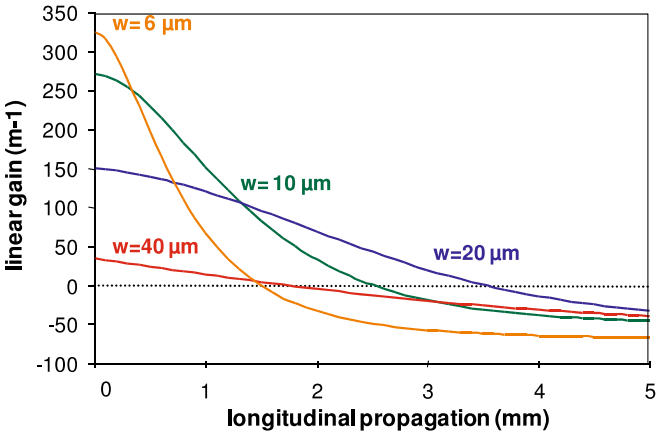

FIGURE 4 Evolution of the small-signal gain with crystal length for different pump waists radii (pump power = 300 mW). The laser and pump waists are assumed to be equal and located at the input of the crystal

w (μm)	L_t (mm)	G			
		$L = 1$ mm	$L = 2$ mm	$L = 3$ mm	$L = 5$ mm
6	1.4	1.48	1.50	1.37	1.06
10	2.5	1.53	1.76	1.73	1.39
20	3.5	1.28	1.51	1.60	1.44
40	1.7	1.01	0.99	0.94	0.77

TABLE 2 Evolution of the transparency length (L_t) and the integrated gain ($G(L)$) with the crystal length L and the pump waist radius (w)

Crystal length (mm)	One pass absorption (%)
5	70
3	50
2	40

TABLE 3 One-pass absorption of our different Nd:ASL crystals

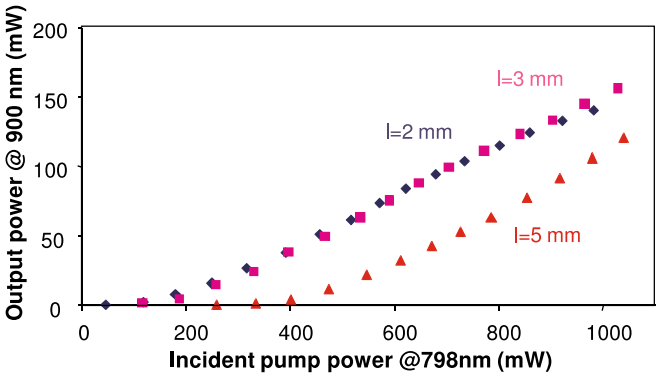

FIGURE 5 Laser power with a 10-μm pump waist radius and a $T = 5\%$ output coupler for different crystal lengths: *triangles* ($l = 5$ mm), *squares* ($l = 3$ mm), *diamonds* ($l = 2$ mm)

where N is the density of neodymium ions in the crystal, σ_{aP} the absorption cross section at the pump wavelength, and τ the fluorescence lifetime. $I_p(r, z)$ is the pump intensity taking into account the Gaussian propagation of the pump beam. σ_{eL} and σ_{aL} are respectively the emission and absorption cross sections at the laser wavelength. $A(r, z)$ stands for the Gaussian profile of the laser mode. The spectroscopic data used are listed in Table 1. The crystal is assumed to be cylindrical with a radius r_c much larger than the beam size. Figure 4 shows the evolution of g_0 along the crystal for different pump waist radii and an incident pump power of 300 mW close to our experimental values of the laser threshold. With a small pump waist (6 μm), the gain is very high at the beginning of the crystal. The large beam divergence causes the gain to decrease very quickly and reabsorption occurs beyond a transparency length of ~ 1.4 mm. In contrast, with a large pump waist, the gain is very low because of the strongly reduced incident pump intensity. The relevant parameter for laser operation is the double-pass integrated gain given by:

$$G(L) = \int_0^L e^{2g_0(z)}\, dz\,, \tag{2}$$

where L is the crystal length. From our simulations, we expect to have the highest gain for a waist radius of 10 μm and a crystal length of 2 to 3 mm (see Table 2).

We first investigated cw laser emission at 900 nm. The experimental setup is presented in Fig. 2. The strong astigmatism of the tapered amplifier was corrected by use of a cylindrical 300-mm focal length lens to both correct and circularize the pump beam. An optical isolator (isolation > 20 dB) is placed at the output of the tapered amplifier to avoid parasitic back-reflections. The pump waist radius is varied by changing the focal length of the focusing lens. We used a 5%-doped Nd:ASL crystal ($Sr_{0.7}La_{0.25}Nd_{0.05}Mg_{0.3}Al_{11.7}O_{19}$, $N \sim 1.7 \times 10^{20}$ cm^{-3}) crystal grown by the Czochralski pulling technique. In order to minimize thermal population of the ground laser level, the copper mount of the Nd:ASL crystal is maintained at 14 °C with a water cooling device. The resonator is a simple plane-concave cavity: the plane mirror (HR 900 nm – HT 800 nm) is deposited on the input face of the crystal, and the output coupler at 900 nm is a 100-mm radius of curvature concave mirror with a high transmission at the pump wavelength. Both mirrors are anti-reflection coated at 1050 nm to prevent laser emission of the intense $^4F_{3/2} \rightarrow {}^4I_{11/2}$ four-level-transition. In order to maximize the gain and avoid reabsorption the overlap between the laser beam and the pump beam has been optimized by setting up the cavity length and the focus position of the pump beam.

Three crystals of different lengths (2, 3 and 5 mm) have been tested. The one-pass absorption of these crystals is presented in Table 3 showing that for the 2- and 3-mm-long crystals, more than 50% of the pump power is not absorbed, as usual in quasi-three level lasers. The shorter crystals result in a significantly lower pump threshold (see Fig. 5) due to the reduced reabsorption of the laser emission and despite the lower pump absorption. Several pump waist radii have been tried:

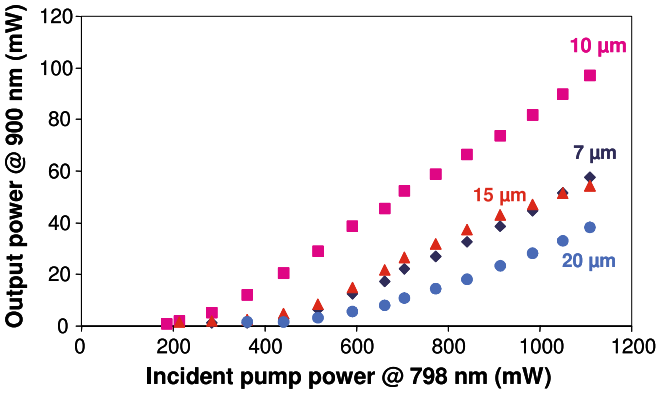

FIGURE 6 Pump waist optimization with a 3-mm-long Nd:ASL crystal and a $T = 10\%$ output coupler: *circles* (20 µm), *triangles* (15 µm), *squares* (10 µm), *diamonds* (7 µm)

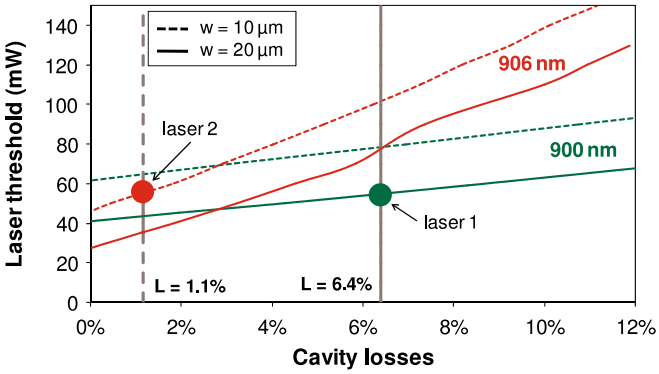

FIGURE 7 Laser pump threshold vs. cavity losses for the two investigated setups: $w = 10$ and 20 µm for the 900 and 906 nm emissions (respectively *green* and *red*). *Green* and *red dots* represent the operating conditions for laser 1 ($w = 10$ µm, $R = 95\%$, $L = 1.1\%$) and laser 2 ($w = 20$ µm, $R = 99.85\%$, $L = 6.4\%$). We assumed 1% of internal losses

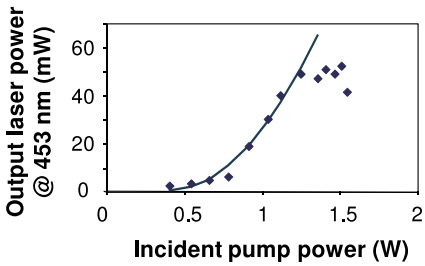

FIGURE 8 SHG performance (*dot* – experimental values; *line* – parabolic fit) vs. incident pump power at 798 nm

7, 10, 15 and 20 µm with a $T = 10\%$ output coupler (Fig. 6). Regardless of the crystal length, the lowest threshold and the highest output power are obtained with a 10 µm pump waist radius corresponding to a $f = 50$ mm focusing lens. Finally, our best results have been obtained with a crystal length of 3 mm, a pump waist radius of 10 µm and a 5%-output coupler: 156 mW at 900 nm for 1.1 W incident pump power at 798 nm. The threshold was as low as 180 mW for a slope efficiency of 34% as a function of absorbed pump power.

4 Intracavity frequency doubling

In order to evaluate the possibility of intracavity frequency doubling of the infrared beam, a laser cavity with a concave mirror highly reflective at the laser wavelength ($R = 99.85\%$) has been implemented. This mirror was also high-reflection coated for the pump ($R = 99.95\%$). The pump and laser waists were set to 20 µm to increase the Rayleigh range. In these conditions, we observed a strong laser emission at 906 nm, corresponding to the transition from the $^4F_{3/2}$ level to the highest Stark sub-level of the $^4I_{9/2}$ level, instead of the 900 nm line previously observed with the 5%-output coupler. Such an effect has already been observed with Nd:$GdVO_4$ laser operating on the same $^4F_{3/2} \rightarrow {}^4I_{9/2}$ transition [15] and with Er:Yb:glass [16]. This red-shift of the laser wavelength with reduced intracavity losses is imputed to the lower absorption cross section at 906 nm as compared to 900 nm, resulting in a lower transparency pump power. This has been confirmed by computing the double-pass gain of both observed laser transitions as a function of pump power, using the spectroscopic data of Table 1. The results are shown in Fig. 7. We consider our two different experimental operating conditions (1 – pump and laser waist radii of 10 µm and a $R = 95\%$ output coupler, 2 – pump and laser waist radii of 20 µm and a $R = 99.85\%$ output coupler). Based on these simulations, it is clear that for cavity 2 with a high reflective mirror, the threshold at 906 nm is lower than at 900 nm. On the contrary with a higher output coupler ($T = 5\%$), the lowest threshold is for the 900-nm emission (laser 1). The output power at 906 nm through the low-transmission concave mirror reached 300 mW at the incident pump power of 1.5 W, corresponding to an intracavity laser power of 200 W.

Second harmonic generation is performed by inserting a LBO crystal into the cavity. The LBO crystal is 15-mm long and cut for type-I phase-matching ($\theta = 90°$, $\varphi = 22.5°$). We place it as close as possible to the Nd:ASL crystal to maximize the intracavity laser intensity. In order to reduce the divergence of the laser beam and match the angular acceptance of the nonlinear crystal (4.41 mrad cm), the pump and laser waists are increased to 20 µm. The temperature of the nonlinear crystal is regulated at 25 °C by a Peltier module to adjust and stabilize the phase matching angle of the LBO. We obtain an output power of 53 mW at 453 nm for a maximum pump power of 1.5 W with the 3-mm long Nd:ASL crystal (see Fig. 8), resulting in an optical-to-optical efficiency of 4%. The blue beam was close to the diffraction limit below 40 mW. It is worth noting that the output power is limited by the degradation of the pump beam quality at high operating current.

5 Conclusion

We have demonstrated the first diode-pumped Nd:ASL laser. This was achieved by developing a high-brightness wavelength-stabilized pump source based on an extended cavity tapered amplifier with a volume Bragg grating (several watts, linewidth < 80 pm, wavelength-locked to the absorption transition). An output power of 153 mW at 900 nm is demonstrated with a 3-mm long crystal; more recently a power of 240 mW was obtained under a higher pump power (1.5 W). With a HR output coupler and with pump recycling, we obtained 300 mW at 906 nm. Intracavity frequency doubling is also performed with a LBO crystal, and

we obtain 53 mW of blue laser emission at 453 nm. These performances compare well with previous results obtained under Ti:sa pumping in the same power range [9]. We believe that these results are an important step on the way to a compact and efficient Nd:ASL blue emitting laser. Moreover, with the new generation of tapered amplifiers with improved beam quality and powers [9], even higher performances should be possible.

ACKNOWLEDGEMENTS The authors thank Gilles Colas and Christian Beurthe from Institut d'Optique for the polishing of the crystals. This work has been partially supported by the European Community under the www.BRIGHT.eu integrated project (IP511722). D. Paboeuf acknowledges the funding of his PhD by the Délégation Générale de l'Armement (France).

REFERENCES

1 T.Y. Fan, R.L. Byer, Opt. Lett. **12**, 809 (1987)
2 P. Zeller, P. Peuser, Opt. Lett. **25**, 34 (2000)
3 Q.H. Xue, Q. Zheng, Y.K. Bu, F.Q. Jia, L.S. Qian, Opt. Lett. **31**, 1070 (2006)
4 Y.D. Zavartsev, A.I. Zagumennyi, F. Zerrouk, S.A. Kutovoi, V.A. Mikhailov, V.V. Podreshetnikov A.A. Sirotkin, I.A. Shcherbakov, Quantum Electron. **33**, 651 (2003)
5 M. Castaing, E. Hérault, F. Balembois, P. Georges, C. Varona, P. Loiseau, G. Aka, Opt. Lett. **32**, 799 (2007)
6 A. Lupei, V. Lupei, C. Gheorghe, D. Vivien, G. Aka, P. Aschehoug, J. Appl. Phys. **96**, 3057 (2004)
7 V. Lupei, G. Aka, D. Vivien, Opt. Lett. **31**, 1064 (2006)
8 C. Varona, P. Loiseau, G. Aka, B. Ferrand, V. Lupei, Proc. SPIE **6190**, 27 (2006)
9 F. Dittmar, B. Sumpf, J. Fricke, G. Erbert, G. Tränkle, IEEE Photon. Technol. Lett. **18**, 601 (2006)
10 M. Kelemen, J. Weber, G. Kaufel, G. Bihlmann, R. Moritz, M. Mikulla, G. Weimann, Electron. Lett. **41**, 1011 (2005)
11 B. Volodin, S. Dolgy, E. Melnik, E. Downs, J. Shaw, V. Ban, Opt. Lett. **29**, 1891 (2004)
12 B. Jacobsson, J.E. Hellström, V. Pasiskevicius, F. Laurell, Appl. Phys. B **91**, 85 (2008)
13 G. Lucas-Leclin, D. Paboeuf, P. Georges, J. Holm, P. Andersen, B. Sumpf, G. Erbert, Appl. Phys. B **91**, 493 (2008)
14 S. Yiou, F. Balembois, P. Georges, J. Opt. Soc. Am. B **22**, 572 (2005)
15 E. Hérault, F. Balembois, P. Georges, Opt. Lett. **31**, 2731 (2006)
16 S. Taccheo, P. Laporta, C. Svelto, Appl. Phys. Lett. **68**, 2621 (1996)